J Nanostruct 16(3): 3786-3806, Summer 2026

RESEARCH PAPER

# Synthesis of Novel Magnetic Chelating Resin and Analytical Study of Its Efficiency in Removing Some Heavy Metals from Their Aqueous Solutions

*Iman Saad Ali* [1], *Raheem Karam Zobon* [2*]

[1] *General Directorate of Basra Education, Basra, Iraq*

[2] *General Directorate of Misan Education, Misan Iraq*

ARTICLE INFO

***Article History:***
*Received 07 February 2025*
*Accepted 15 April 2026*
*Published 01 July 2026*

***Keywords:***
*Adsorption*
*Composite resins*
*Isotherm*
*Metal ions*
*Nanomaterials*

ABSTRACT

With the application of a phosphorylation polycondensation, a new azomethine-containing carboxylic acid monomer (5-aminoisopthalic acid) was converted with aromatic diamines to a novel magnetic poly (azomethine amide) (P5A-P). FT-IR, 1H-NMR, and 13C-NMR spectroscopic analysis were used to make the characterization. The co-precipitation approach was also used to create magnetic nickel iron oxide, $NiFe_2O_4$, which was subsequently impregnated with prepared resin. The particle sizes of the nickel, iron oxide, and magnetic resin composite were found to range from 22 to 36 nm. The composition was characterized using X-ray diffraction, and the analytical efficiency was investigated using batch adsorption and flame atomic absorption. The polyamides were found highly effective at removing $Cu^{2+}$, $Cd^{2+}$, and $Pb^{2+}$ metal ions from their aqueous solutions, and the order of selectivity in the mixture of these ions was $Pb^{2+} > Cd^{2+} > Cu^{2+}$. The Freundlich equation was found to be more in agreement with the adsorption process. The high correlation coefficient ($R^2$) and the agreement between experimental and calculated values of the adsorption capacity showed that the Pseudo-second-order model best fit the experimental data for the studied ions. The novelty of this study is evident in the design of a new monomer, which has not been previously used in the preparation of magnetic resins, as well as the incorporation of azomethine bonds within a magnetic polyamide structure, which improved the adsorption efficiency and selectivity of the new resin towards the studied metal ions.

**How to cite this article**
*Saad Ali I, Karam Zobon R . Synthesis of Novel Magnetic Chelating Resin and Analytical Study of Its Efficiency in Removing Some Heavy Metals from Their Aqueous Solutions. J Nanostruct, 2026; 16(3):3786-3806. DOI: 10.22052/JNS.2026.03.066*

## INTRODUCTION

Water pollution is becoming more prevalent due to the rapid growth of industrial and agricultural activities, despite strict regulations to control it, jeopardizing human health and environmental safety. Significant attention is currently being directed towards the problem of heavy metal ion pollution [1,2].

* *Corresponding Author Email: r.k.alsaidi@gmail.com*

The success of the adsorption process depends on the performance of the adsorbent material. The cost of the wastewater treatment system is taken into consideration when selecting a treatment technology, and adsorption technology is known for its low cost [3-5]. Additionally, this method is easy to use, making it a top choice for treating wastewater containing heavy metals.

**This work is licensed under the Creative Commons Attribution 4.0 International License.**
To view a copy of this license, visit http://creativecommons.org/licenses/by/4.0/.

Furthermore, when choosing a wastewater treatment technology, it's important to consider that adsorption has a high adsorption rate (maximum removal rate of 99%) and a high adsorption capacity compared to other methods.

Because of their exceptional thermo-mechanical qualities and high chemical stability, aromatic polyamides are engineered polymers and suitable adsorbents for heavy metal ions, and their stability allows them to be used in water under a variety of temperatures and environmental conditions. Polyamides tend to retain water due to the presence of amide groups. Water absorption and ion exchange properties can be improved by modifying the material's hydrophilicity by adding regular amounts of sulfonic acid groups to the polymer main chain. Improving the hydrophilicity of the polymer to enhance water absorption also facilitates access to adsorption sites, enhancing the ability to adsorb heavy metals. Given their potential use in water treatment, polyaramids are of great interest [6,7].

Taking into account the cost of treatment equipment the adsorption by resin has a high adsorption rate, a large adsorption capacity, and a maximum removal rate of 99% when compared to other methods. It has the benefits of being inexpensive and having an easy-to-use operation approach. The primary chain of chelating resins is often a crosslinked polymer, a kind of polymer material that has been grafted with functional groups to give it unique properties. It is essentially a type of polymer material featuring chelating groups for O, N, S, and P. Chelating resins have superior adsorption selectivity as compared to conventional small molecule chelating agents. Additionally, the three-dimensional molecular structure and the chelating resin body structure's molecular framework are insoluble in water [8,9].

Magnetite nanoparticles have attracted a lot of attention due to their exceptional physicochemical properties, especially their strong magnetization, unique electrical characteristics, large surface area, small size, and high adsorption capacity. They can be easily separated from water using an external magnetic field, and various polymers can be used to functionalize their surface. Several of polymeric coatings and surfactants are widely used, making them a great option for wastewater treatment because of these special qualities. One of the most significant spinel ferrites is nickel ferrite ($NiFe_2O_4$). Its distinct magnetic structure, high magneto

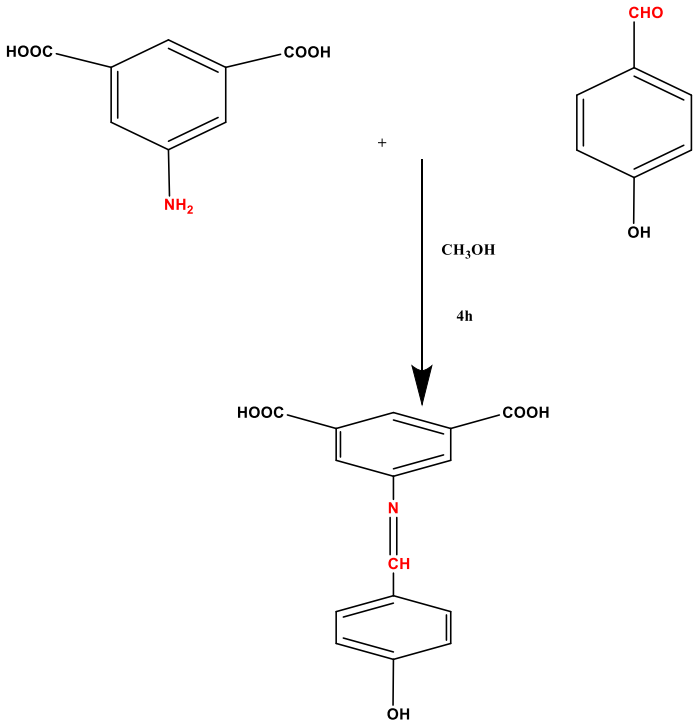


Fig. 1. Preparation path of the Schiff base [5A-P].


CC BY

crystalline anisotropy, and notable saturation magnetization are what particularly interest researchers. The size and form of the particles determine whether $NiFe_2O_4$ shows ferrimagnetic, superparamagnetic, or paramagnetic activity [10].

Nanomaterials come in a variety of forms and are created using polymers. They have performed exceptionally well in environmental remediation, particularly in the treatment of water. Because of their many dimensions, unique activities, and great potential, polymeric nanomaterials are amazing. They work especially well for treating water that has been contaminated by heavy metals [11]. The effectiveness of various nano polymers, such as sheets, needles, and beads, in eliminating heavy metal ions from water varies. Due to the porosity of resins, the nano polymer was created from salts of metal nanoparticles and typically functioned as adsorbents in wastewater [12,13]. Magnetite nanoparticles in combination with polymers were shown to exhibit the strong adsorption characteristics [14].

Several recent studies have demonstrated the significant importance of $NiFe_2O_4$/polymer composites in removing metal ions. For example, Khalaj et al. [15] successfully prepared $NiFe_2O_4$@$SiO_2$ nanoparticles doped with polyethyleneimine (PEI) for the removal of $Cr^{6+}$, $Ni^{2+}$, and $Pb^{2+}$ ions, demonstrating excellent adsorption and usability. Fadel et al. (2024) also used a chitosan polymer to prepare an effective Chitosan–$NiFe_2O_4$ composite in wastewater treatment, confirming that the integration of diverse materials and biopolymers adds to the small particles. Satyanarayana and Akhron (2022) also combined $NiFe_2O_4$ with conductive materials such as graphene, giving the composite additional functional properties and potential advantages in advanced applications

A recent review by Kumar and Onion [18] also discussed the use of branched polymer composites for the removal of metal ions. This approach, which cannot be relied upon to improve

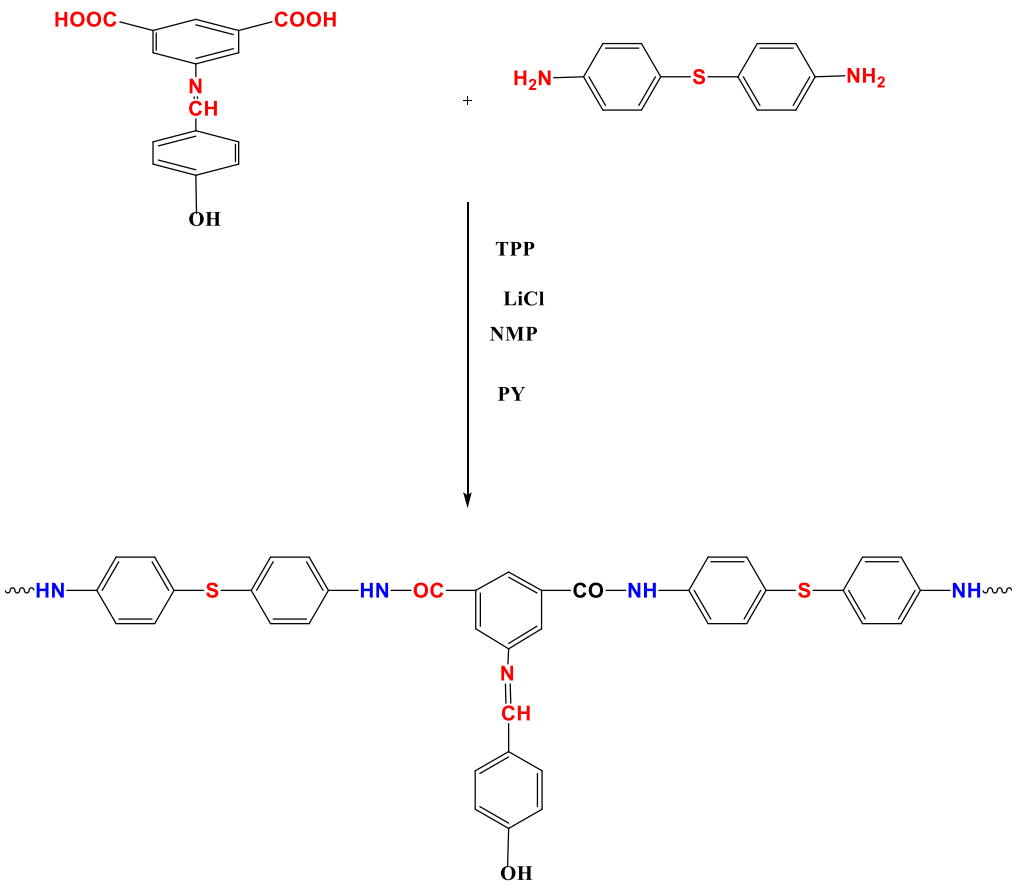


Fig. 2. Preparation route of chelate resin [P5A-P].

the synergistic interaction between the polymer and the differentiated material, is an effective and environmentally friendly method [15- 18].

Thus, in this context, this study focuses on the preparation of a polymer/$NiFe_2O_4$ composite using a simple co-precipitation approach, while evaluating its structural and magnetic properties and adsorption mechanism. This work differs from previous studies in that it utilizes a low-cost and manufacturing method, with a detailed analysis of the composite formation mechanism and a study of the synergy between polymer and ferrite in removing heavy metals from wastewater.

## MATERIALS AND METHODS

*Materials*

Without any additional purification, all chemicals and solvents were purchased from reputable commercial sources like Sigma-Aldrich and Merck and were ≥99% pure.

*Instrumentation*

This work was accomplished using a variety of instruments, which are listed below: Shimadzu, Japan's FT-IR 8400S was used to measure. FT-IR spectra, X-ray diffraction (XRD) equipment (type: Philips, PW1730), scanning electron microscopy (SEM) pictures, and energy-dispersive X-ray (EDX) employing Zeiss microscopy at 10.00 Kv were utilized. Surface area was evaluated at 450ºC under $N_2$ gas as an adsorptive analysis on BEL, model BEL SORP MINI II, Japan; mass spectrum was measured using the EI technique; and Agilent technology (HP) H-NMR and 13C-NMR spectra were performed on a Bruker DRX (500 MHz and 100 MHz, respectively).

*Preparation of Schiff base [5A-P]*

Reflux distillation was performed for four hours after (2.1g, 0.01mol) of amine (5-Aminoisophthalic acid) was added after being dissolved in 40 ml of methanol to (g1.22, 0.01mol) of aldehyde (4-Hdroxybenzaldehyde) diluted in (10ml) of methanol. The reaction progress was monitored using Thin Layer Chromatography (TLC). After filtering the reaction mixture and allowing it to cool, an orange-yellow precipitate appeared. It was recrystallized in a solution of water and DMF after being filtered and dried in a drying oven [19]. The yield was 85% and its melting point was (301-302°C).

*Nuclear magnetic resonance spectrum (1H-NMR1), infrared spectrum (FT-IR), elemental analysis (C.H.N.), and diagram were all captured*

FT IR (KBr, $cm^{-1}$): 3428 (m), 3086 (m), 1700 (s),

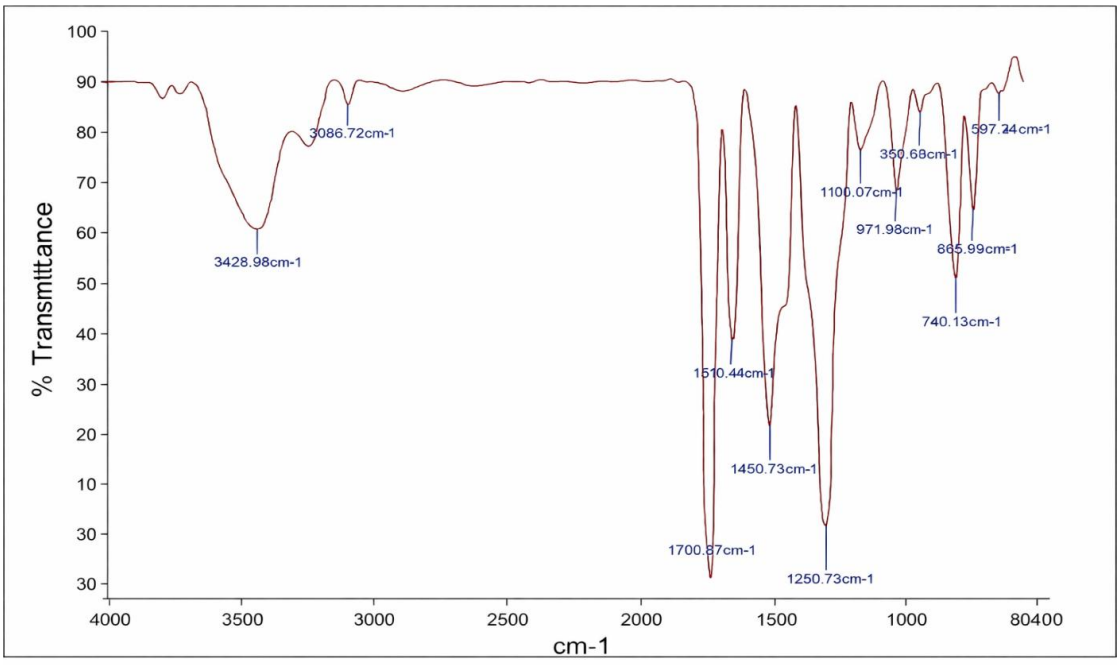


Fig. 3. FTIR spectra of 5A-P.

1610 (s), 1281 (s), 1247(s), 1106 (w). d.t. 312-313 °C. 13.4 (m, 2H, COOH), 12.6 (s, 1H, OH), 10. 1 (s, 1H. -CH=N-), are the 1H NMR (DMSO-d6, d, ppm) values. 190. (C1), 167.1 (C2), 163.2 (C2), 149.2 (C3), 113-130- (C5,8,6,9) are the 13C NMR (DMSO-d6, d, ppm) results. For $C_{15}H_{11}NO_5$, the elemental analysis yielded the following results: C, 63.11. %; H, 3.89%; N, 4.91%; O, 28.04. %, Found: C, 62.98%; H, 3.99%; N, 4.89%, O,28.13%.

The prepared Schiff base suggested chemical structure is displayed Fig. 1.

*Preparation of chelate resin [P5A-P] for Schiff base [5A-P]*

The reaction system consists of a three-necked round-bottom flask with a magnetic stirrer, a condenser, and an addition port attached. After adding 5 mmol of Schiff base (5A-P), 5 mmol of 4,4-thiodianilin SDA, 0.5 g of lithium chloride, 3.1 g 10 mmol of triphenyl phosphite, 2.5 ml of pyridine, and 10 ml of N N-methyl-2-pyrrolidone (NMP), the mixture was heated to 100 °C under nitrogen gas for 10-8 hours. When the reaction was complete, a soft gel was formed. The product was filtered out, cleaned with hot methanol, and dried at 80 °C after the viscous mixture was added to methanol. Fig. 2 provides the chelate resin [20].

*Preparation of magnetic Nickel iron oxide*

The $NiFe_2O_4$ NPs sample was made by dissolving 4 g of Fe $(NO_3)_3.9H_2O$ and 2 grams of Ni $(NO_3)2.6H_2O$ in 100 ml of deionized water. After that, the mixture was continually agitated for two hours at 80 degrees using a magnetic stirrer. To extract the precipitants, the mixture was centrifuged at 4000 rm after being stirred and repeatedly washed with deionized water. The finished product was dried for six hours at 100 degrees in an electric oven and then heated to 700 degrees for two hours in an open-air furnace [19].

*Preparation of magnetic Nickel iron oxide composite resins*

In a 500 ml flask with $N_2$, 200 ml of N-methyl-2-pyrrolidone (NMP) was used to dissolve 0.6 g of aromatic polyamide. Over the course of 60 minutes, the 100 ml $NiFe_2O_4$ nanoparticle/NMP suspension that had been previously made was progressively added to the polymer solution. To precipitate the magnetic particles, the suspension was placed on a neodymium magnet after being shaken for a whole day at room temperature. After that, NMP was used to clean the magnetic particles until there was no more polymer in the supernatant solution. After another methanol wash, the particles were vacuum-oven dried at ambient temperature [21].

## RESULTS AND DISCUSSION

*FTIR*

The stretching of the implicit hydrogen bond that forms between the proton of the hydroxyl group and the electron pair of the nitrogen atom

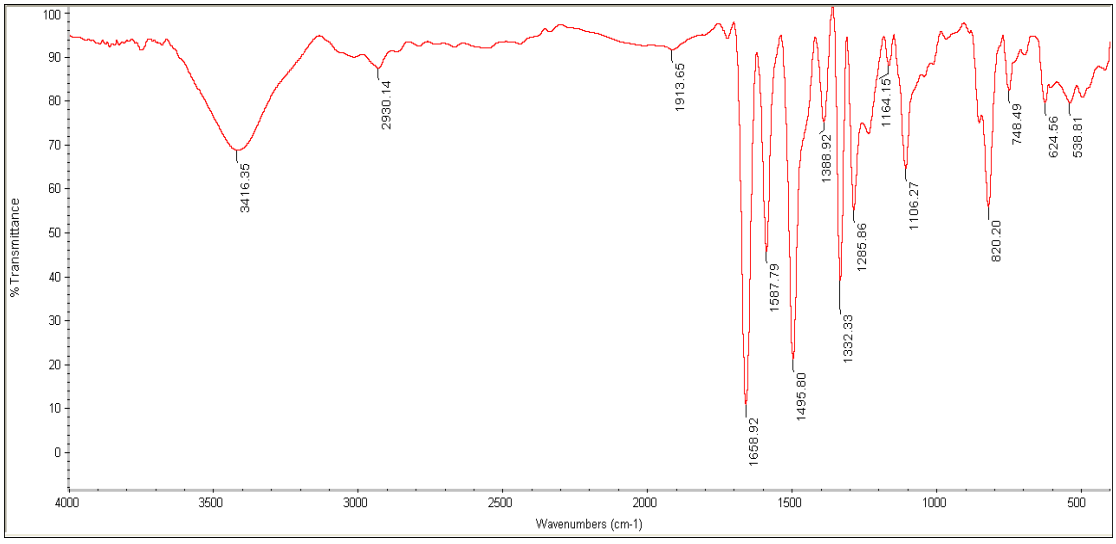


Fig. 4. FTIR spectra of P5A-P.

and the azomethine group was identified as the cause of the weak stretching band in the ligand spectrum in the compound under investigation, which was observed in the frequency range 3428 $cm^{-1}$. The aromatic (C-H) vibration frequencies are responsible for the weak stretching band that was also detected in the range of 3086 $cm^{-1}$. According to the literature, the spectrum also showed two strong stretching bands: one in the frequency range (1610) $cm^{-1}$, which was attributed to the

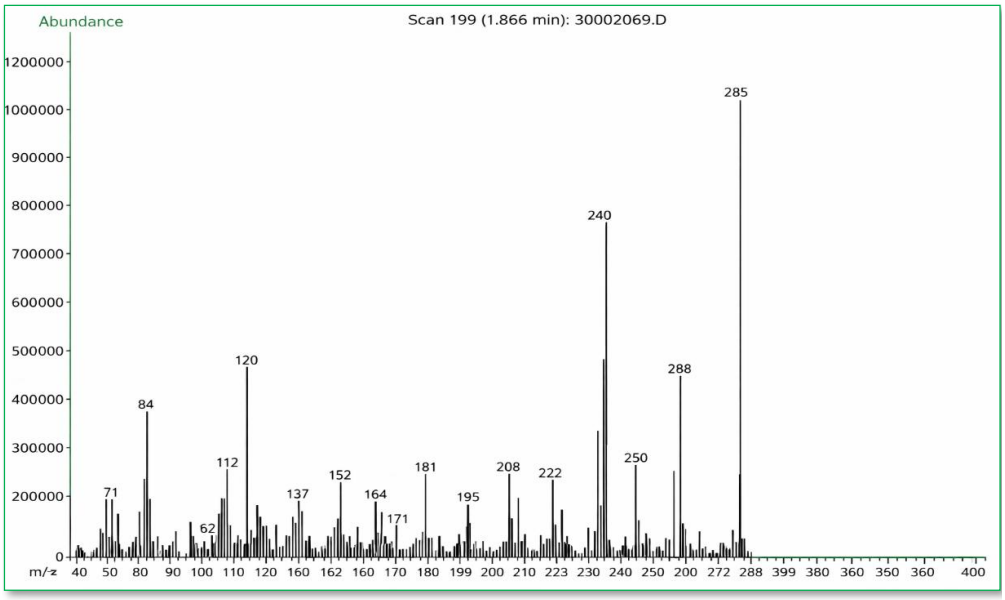


Fig. 5. mass spectra of 5A-P.

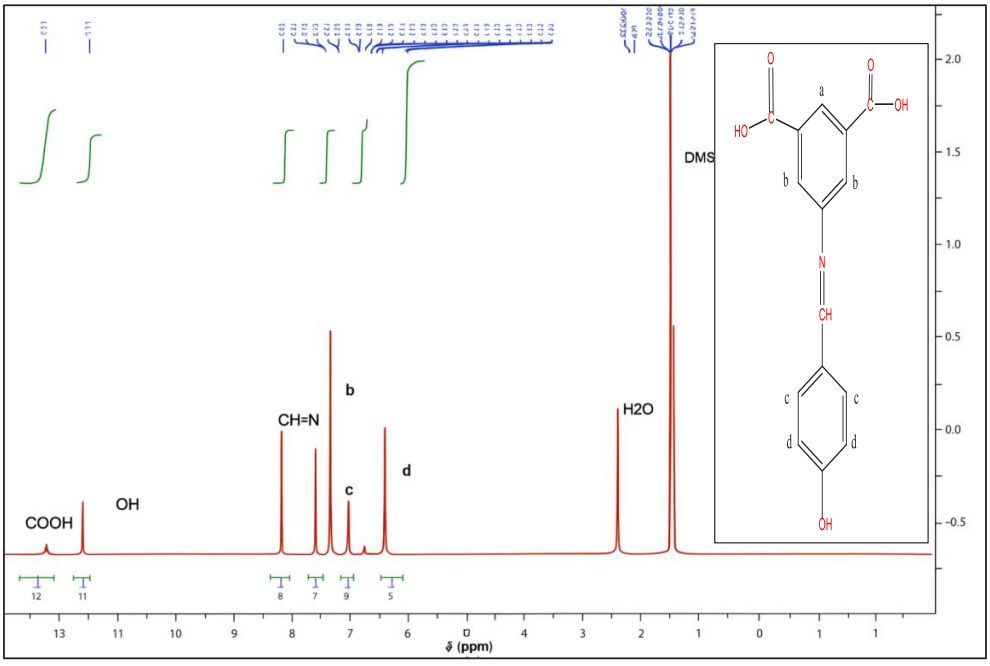


Fig. 6. 1H-NMR spectrum of 5A-P.


CC BY

azomethine group, and the other in the range of (1700) $cm^{-1}$, which was attributed to the carboxyl group's (C=O) bond. The range between (1247) $cm^{-1}$ was also where the (C-N) bond's stretching frequency was observed. While the phenolic hydroxyl groups in the area between (1207) $cm^{-1}$ are responsible for the stretching frequency of the (C-O) bond, because of hydrogen bonding, a new broad band is seen in the corresponding resin. Additionally, the creation of the amide bond is indicated by the shift of the aromatic amine's carboxyl group band to lower frequencies (1658) $cm^{-1}$ [22]. Additionally, in the range, the azomethine group is moved to lower frequencies (1587) $cm^{-1}$.

The outstanding adsorption performance of the produced material (P5A-P) is directly associated with its surface and structural characteristics, according to the spectral and structural characterization of the material. Azomethine bonds (–CH=N–) and amide groups (–CONH–) were verified by FTIR and NMR spectra, suggesting the presence of active sites that can form hydrogen or coordination interactions with pollutant molecules. The material's great selectivity towards ions or dyes is attributed to these sites, which is in line with research on azomethine-containing polymers that have shown remarkable adsorption capability because of the presence of electron-donating bonds.

The Schiff base monomer's infrared spectrum and the resin made from it are displayed in Figs. 3 and 4.

The chemical formula of the Schiff base compound (5A-P) was established by recording its mass spectra. Along with a collection of splitting peaks of varying molecular weights that varied in their relative abundance, such as the fragmentation peak at m/z = (240), which is caused by the molecular ion after losing the carboxyl group (COOH) with a molecular weight of (45), the aforementioned spectrum in Fig. 5 displayed the partial ion peak (M+.) representing the basic ion with a relative abundance of 100% at M/Z = 285 for the monomer 5A-P.

The compound [5A-P] in Fig. 6 1H-NMR spectrum displayed a signal at (13.4 δ) ppm from the carboxylic OH proton and a signal at (12.6 δ) ppm from the phenolic OH proton and the phenolic OH proton in the para position. The -N=CH- proton in the 10.1) ppm position also produced a signal, and the protons of the aromatic ring produced a multiple signal at the ppm position (δ 8.4-6.9) ppm.

Fig. 7 displays the 13 C-NMR spectra of the Schiff bases made with dimethyl sulfoxide (DMSO-d6) solvent. We see the following from the C-NMR 13 spectroscopic study: The carbon atom

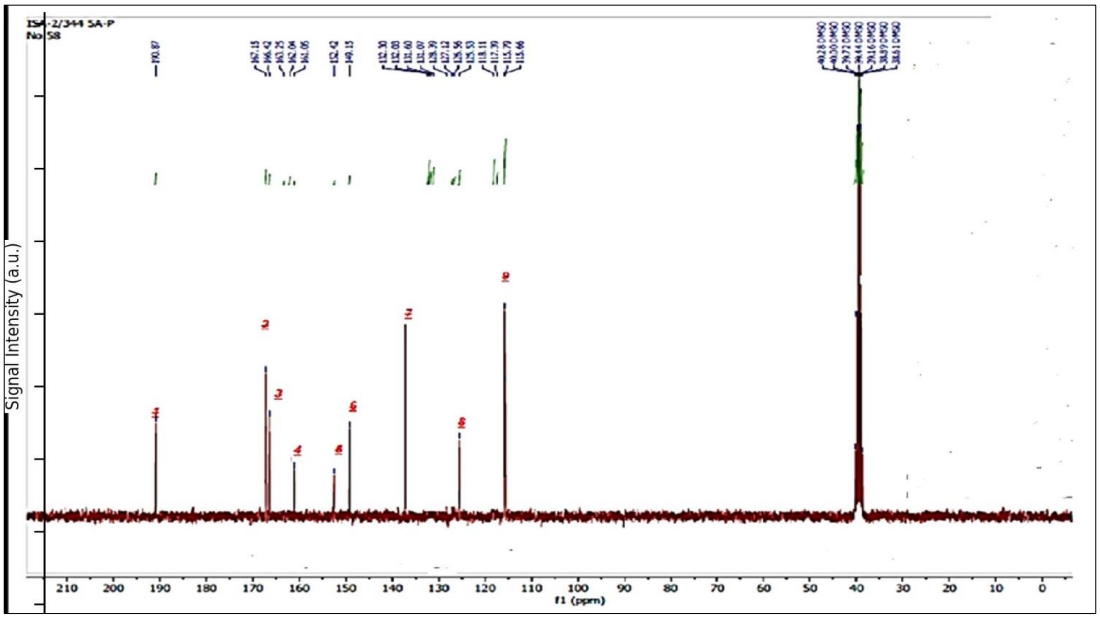


Fig. 7. 13C NMR spectrum of 5A-P.


CC BY

of the carboxyl group and the carbon atom of the carbon group connected to the hydroxyl group are responsible for the signals at the chemical shift (190) ppm and 167) ppm, respectively, in the spectrum of each of the ligands (5A-P). It was further distinguished by the emergence of a signal at (163) ppm, which is caused by the azomethine group's carbon. In addition to the signal of the carbon atoms of the DMSO solvent appearing at (40) ppm, the signals that are caused by the carbon atoms of the aromatic rings also occurred in the range of (115–132) ppm [23]. Figs. 6 and 7 demonstrate this.

The thermal stability of the polymer (P5A-P) was investigated using TG/DTG, and the weight loss curve is shown in Fig. 8. It was found that the P5A-P's initial weight loss was almost at 271.84 degrees C, indicating the polymer's exceptional thermal resilience. The degradation process in air, showing a single primary weight loss (amid link) range is depicted by the two-stage weight loss graph. At 810.48 degrees Celsius, the second stage of weight loss, the azomethine group is evidently broken down. [23].

XRD Fig. 9 displays the XRD pattern of $NiFe_2O_4$ NPs produced by co-precipitation. Without any extra impurity peaks, the x-ray pattern shows the creation of the spinel phase structure of $NiFe_2O_4$. According to standard (JCPDS Card No.74-2081) indexing, the diffraction peaks appeared at

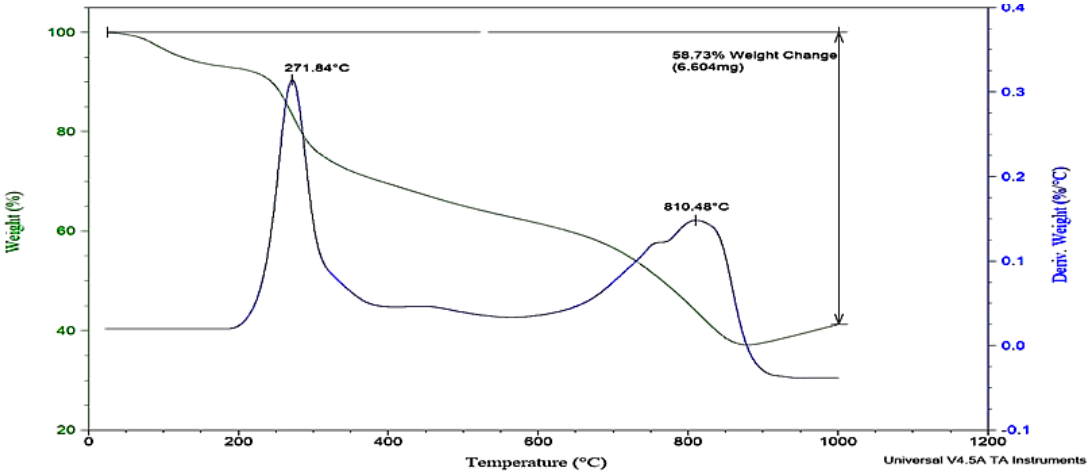


Fig. 8. TGA/DTG thermograms of P5A-P.

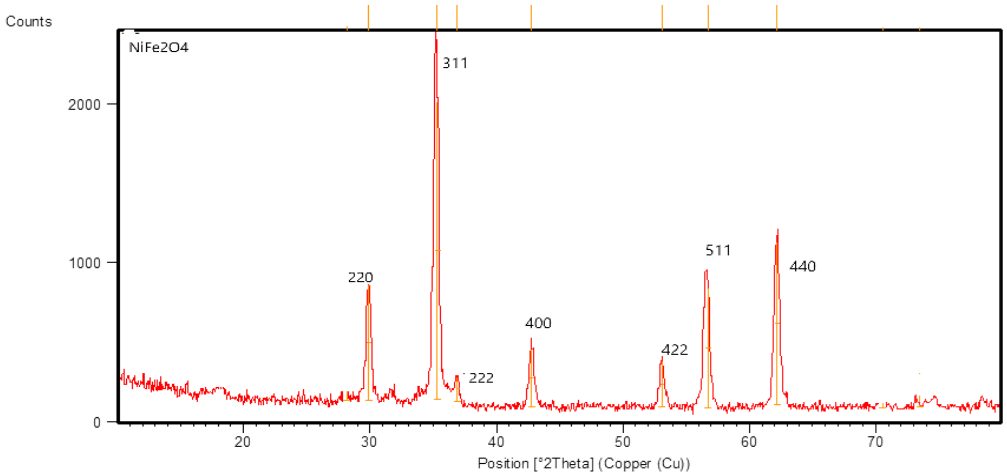


Fig. 9. X-ray diffraction spectrum of sample pure $NiFe_2O_4$.


CC BY

diffraction angles $2\theta$ = 30.295◦, 35.686◦, 37.330◦, 43.375◦, 53.820◦, 57.377◦, and 63.015◦ to (220), (311), (222), (400), (422), (511), and (440), respectively, and correspond to the spinel structure of $NiFe_2O_4$. The entire width at half maximum can be used to estimate the average crystallite size. (FWHM) of the XRD pattern's principal diffraction (311) peak using the Debye Scherrer equation $D = K\lambda\ \beta cos\theta$ (1), where $D$ is the X-ray wavelength (1.5418 Å, Cu Ka), $\beta$ is the peak's FWHM, $\theta$ is the Bragg angle, and $D$ is the average crystallite size in Å. By replacing the value of (FWHM) of the most intense peak (311) in the Scherrer equation, the average crystallite size for the produced $NiFe_2O_4$

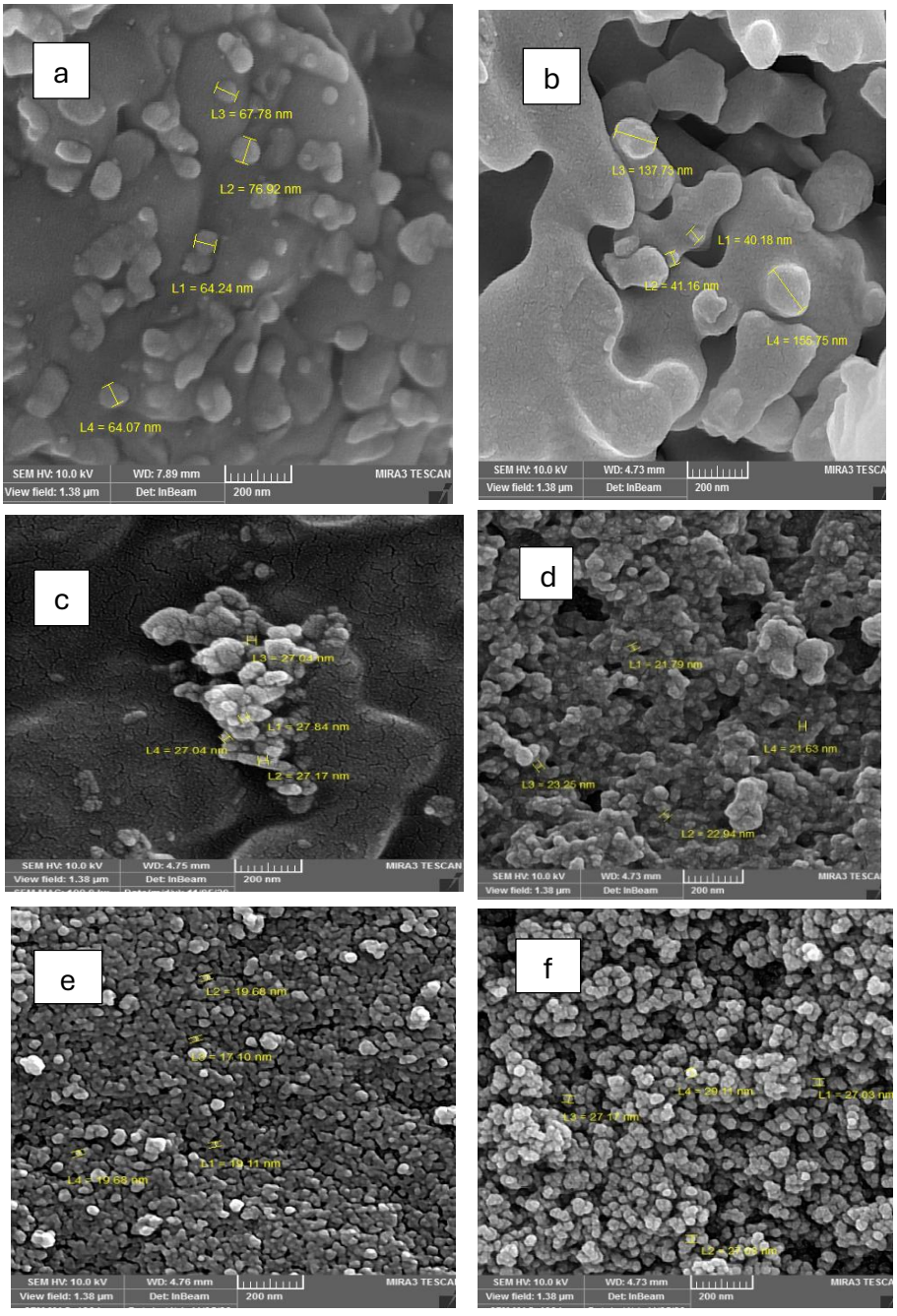


Fig. 10. SEM image (scale bar: 200nm) of (a,b) P5A-P, (c,d) P5A-P/$NiFe_2O_4$, (e,f)$NiFe_2O_4$.

NPs was determined to be 19 nm.

The standard formula $a = \lambda \vee h2 + k\ 2 + l$ (2) $sin\theta$ can be used to determine the lattice constant for the inverse spinel phase structure of the synthesized $NiFe_2O_4$ NPs. In this formula, $a$ stands for the lattice constant, $\lambda$ and $\theta$ represent the x-ray wavelength and Bragg diffraction angle, respectively, and $h$, $k$, and $l$ indicate the miller indices. Using the maximum intensity peak (311) position in Eq. (2), the lattice constant for the synthesized $NiFe_2O_4$ NPs was determined to be 8.1 Å, which is comparable to the method used to determine the average [24].

The incorporation of the magnetic core within the polymer structure without compromising its chemical order was confirmed by XRD measurements, which showed a crystalline phase with peaks corresponding to iron oxides ($NiFe_2O_4$). In keeping with earlier research showing that the presence of a distributed magnetic phase in the polymer matrix strengthens the material's durability and improves its reusability, this crystalline phase leads to improved mechanical stability and uniform particle dispersion.

The SEM pictures of P5A-P (a, b), P5A-P–$NiFe_2O_4$ composites (c, d), and $NiFe_2O_4$ (e,f) particles are displayed in Fig. 10. It is evident that the P5A-P and P5A-P–$NiFe_2O_4$ composites exhibited a strongly agglomerated granular-like appearance. Conversely, $NiFe_2O_4$ particles exhibit a shape that

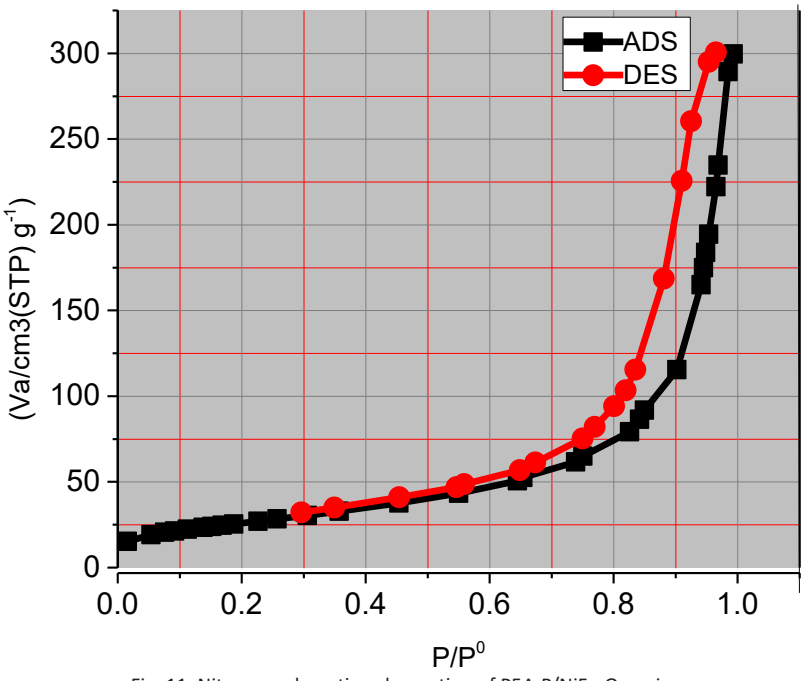


Fig. 11. Nitrogen adsorption-desorption of P5A-P/$NiFe_2O_4$ resin.

Table 1. Surface area and pore volume P5A-P/ $NiFe_2O_4$.

| Property | P5A-P/ $NiFe_2O_4$ |
|---|---|
| Surface area ($m^2/g$) * | 102.539 |
| Pore volume ($cm^3/g$) ** | 0. 432 |
| Pore diameter (nm)** | 17.04 |
| Isotherm type | mesopores |
| Type of Pore | IV |


CC BY

is somewhat round. Similar to P5A-P, the granular morphology of P5A-P–$NiFe_2O_4$ composites shows that P5A-P polymer chains encircle the ferrite particles. To put it another way, the polymerization process coats the surface of $NiFe_2O_4$ particles.

The hydrogen bonding theory for the formation of the ferrite/P5A-P composite was proposed by several studies that demonstrated the well-established behavior of polymer metal oxide composites. They clarified that the twisting of hydrogen bonds between P5A-P chains creates the network topology. The interaction between P5A-P and the oxygen atoms in ferrite causes ferrite particles to become embedded on the P5A-P chain [25].

The material features a rough, uniform porous surface that offers a wide surface area and more active spots, according to SEM pictures. BET measurements, which demonstrated an appropriate surface area and the existence of mesopores with values within the recognized range for similar magnetic adsorption materials (usually between 50–200 $m^2/g$) validate this advanced porous structure. In comparison to several traditional polymers with smaller surface areas, these values show that the new material has a high adsorption capacity for large molecules.

By employing an automated analyzer to quantify the specific surface area of compounds by multilayer $N_2$ adsorption as a function of relative pressure, Brunauer-Emmett-Teller (BET) surface area analysis offers a precise evaluation. This method provides crucial information for adsorption processes as well as assessments of the exterior and pore areas to calculate the total surface area in m2/g. Using adsorption and desorption methods, Barrett-Joyner-Helena (BJH) analysis may also be used to calculate pore volume and specific pore volume. Because of the compounds' particle sizes, this method separates the pore size distribution from the exterior area. Magnetic nickel iron oxide powder and resin (P5A-P/$NiFe_2O_4$) are shown in Fig. 11.

According to the International Union of Pure and Applied Chemistry's (IUPAC) classification and the figures displayed, it was discovered that the adsorbent belong to the fourth class. For this isotherm, the hysteresis loops fall between P/Po<0.9> 0.3 of type 3H, indicating that the surface has irregular porosity in the form of slit-shaped cracks. The mesoporous pores contain the polymer surface pores. Additionally, the BJH method was used to obtain the pore size distribution.

The adsorbent exhibit behavior that is comparable to that of the fourth class, as seen in the aforementioned figures, which further suggests the presence of mesoporous materials. In addition to the impact of pore size and surface area, the absorption of these adsorbents may also be influenced by the size of their particles. The specific surface area, pore volume, and pore diameter of additional produced adsorbents are displayed in Table 1. The pore size of magnetic iron oxide was lower than the surface area of other manufactured adsorbents, and it was found that the $NiFe_2O_4$ adsorbent had a larger surface area than other adsorbents. However, its adsorption capabilities were higher than those of the $NiFe_2O_4$ adsorbent, possibly as a result of the produced resins' larger pore diameters than iron oxide. Thus, it can be said that the interactions between the heavy metals and adsorbents and the functional groups of $NiFe_2O_4$ molecules took place on the surface. However, other adsorbents' active sites within their pores were readily accessible to heavy element ions, which produced favorable outcomes for the adsorption capabilities overall.

The vibrating sample magnometer (VSM) was used to characterize the magnetic properties of the materials. The magnetic nanoparticles of iron oxide and the polymer composites showed superparamagnetic behavior. The saturation magnetization value of Nickel iron oxide was 72emu/g at 300 K. Moreover, the polymer composite magnetic particles showed saturation magnetization values ranging from (66 ) emu/g for polyisomethane-amide resin,. Fig. 12 illustrate this. Although the composite polymer have lower magnetization values, they have sufficient superparamagnetic response to meet the need for separation, as the typical S-shape is shown. Magnetism can disperse the composite polymer particles without agglomeration in solution. The values for magnetite NPs in the literature vary from 42 to 94 emu/g depending on the particle size [27].

According to VSM analysis, the produced material has moderate magnetic characteristics (Ms values between 10 and 70 emu/g), which are adequate for quick magnetic separation following adsorption. Compared to some non-magnetic adsorbents that necessitate intricate physical separation procedures, this is a useful benefit. High adsorption performance and ease of recovery


CC BY

are thus combined in the current material, a qualitative benefit that some researchers have also found in hybrid magnetic polymer materials.

Because zeta potential is utilized to identify the surface charge of P5A-P/$NiFe_2O_4$ and these values are used to determine the stability of the prepared models, the DLS device analyzed zeta potential. good voltage values show good stability and no agglomeration, whilst low values show low stability. This technique was used to determine the sizes and measure the charge of the constructed model. The study's findings as shown in Fig. 13, demonstrated that the composite polymer's zeta potential value in azomethine-amide resin was

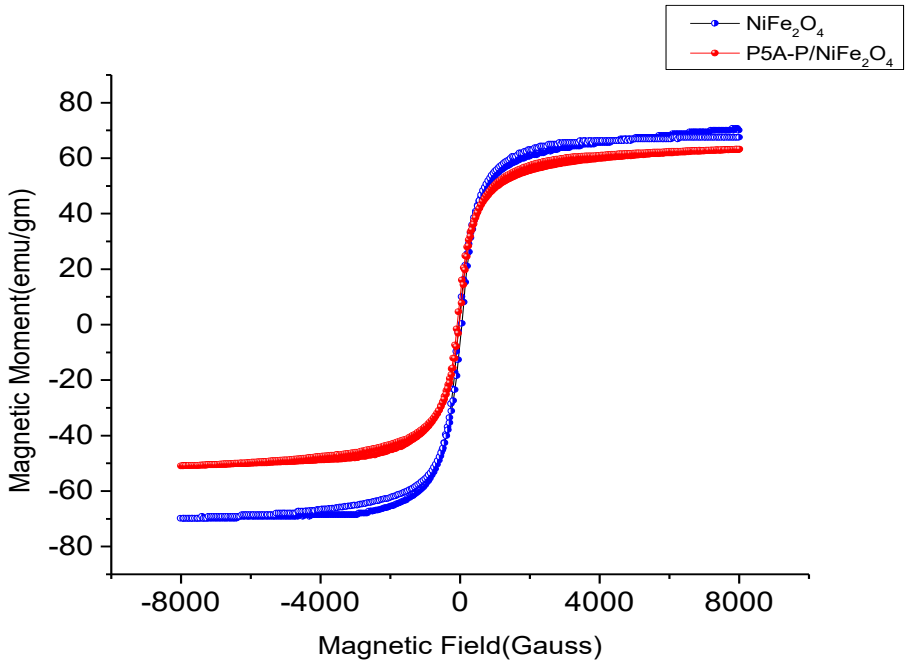


Fig. 12. Field dependence of magnetization for the $NiFe_2O_4$(a) and aromatic P5A-P/$NiFe_2O_4$ nanocomposite(b).

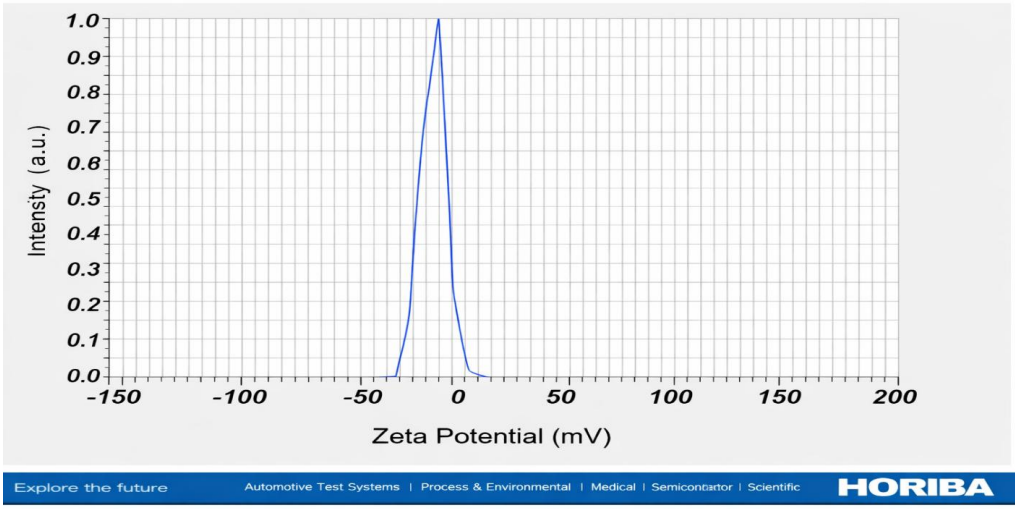


Fig. 13. Zeta potential. 0F P5A-P/$NiFe_2O_4$.


CC BY

-42, indicating that the resins have a negative surface [26].

*TEM and DLS measurements*

The primary determinants of particle size are hydrodynamic diameter and particle size. The particles' size, shape, and hydrodynamic radius were ascertained using dynamic light scattering (DLS) and transmission electron microscopy (TEM), as shown in Figs. 14 and 15a and b. The hydrodynamic radius of the nickel iron oxide nanoparticles was 133.5 nm, and their size was 20.7 nm. Monodisperse distribution was indicated by the polydispersity value of 0.231. The hydrodynamic diameter measures the size of particles in a liquid, where the particle is encircled by various ionic layers of solvents bound in the solution, as opposed to TEM, which measures the size of particles in the dry state. The particles in the solution have a size that is significantly bigger

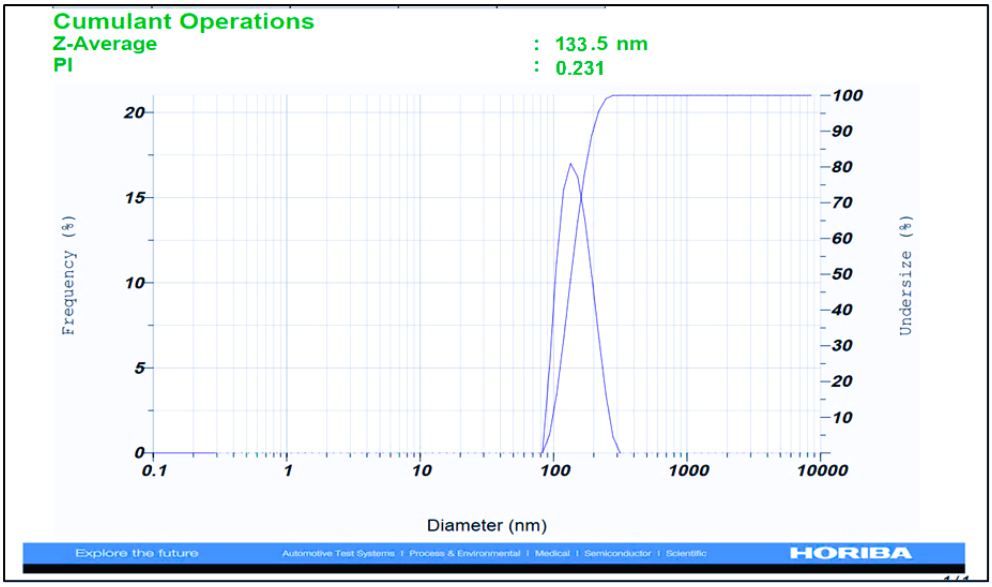


Fig. 14. Dynamic light scattering (DLS). 0F P5A-P/$NiFe_2O_4$.

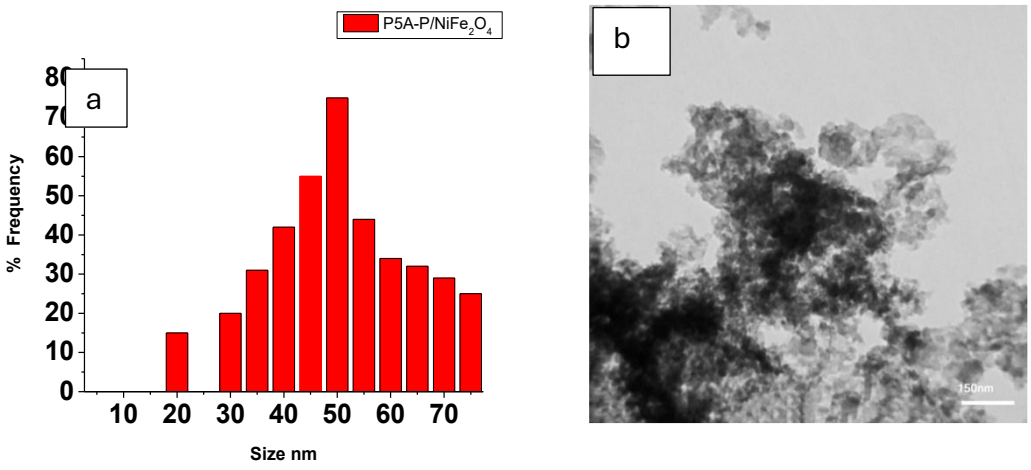


Fig. 15. (a)The particle size distribution of P5A-P/$NiFe_2O_4$ resin, as determined by histogram analysis, showing the dominant particle size range and distribution (b) A TEM image of P5A-P/$NiFe_2O_4$ resin showing the morphological structure and the nature of nanoparticle aggregation within the material.


CC BY

than what the TEM can measure because of their random Brownian motion caused by their many interactions with other particles and solvent particles. [27,28].

The DLS results demonstrate a tight volumetric distribution and hydrodynamic volume at the nanoscale, which facilitates the quick diffusion of adsorbates to effective locations, supporting the stability of the particles in suspension. These results, which show improved homogeneity and a fast adsorption capability, are comparatively lower than those reported for several comparable materials in the literature.

*Analytical method and measurements*

*Preparation of standard solutions*

Standard stock solutions for metal ions were prepared in a volume of (500) ml, by dissolving the necessary weights of metal nitrates in the least possible amount of concentrated nitric acid or concentrated hydrochloric acid, about (1-2) ml, then completing the necessary volume with deionized water.

Then, standard solutions with a concentration of 100 ppm and different acid functions were prepared from the standard stock solutions according to the working pH range for each metal ion and in a volume of 250-500 ml as needed.

In this study, the batch method was used, where (0.01) g of resin was taken and (10) ml of the solution of the metal ion with a concentration of (100 ppm) was added to it, at a pH range of (2-7) based on the pH at which the metal ion begins to precipitate.

The treatment mixture was shaken for different time periods (0.25, 0.5, 2, 4, 24) hours using an electric shaker at a constant speed of (150 rpm) and a constant temperature of (25 °C) for all treatments, then the solutions were filtered, and the concentration of the metal ion in the filtrate was determined by measuring its absorbance using flame atomic absorption spectroscopy expressed as (FAAS). The resin loading capacity is derived from the following relationship:

(L.C) Loading capacity (mg ion/g resin) = [(C) Concentration of the metal ion bound to the resin (mg/L) or (ppm)] * [(a) Conversion factor of the weight used to (1) g] * [(V) Volume of the aqueous solution of the metal ion added to the resin estimated in liters or in the following formula [29-31]:

$$\text{L. C}\left((\text{mg ion}) / (\text{g resin})\right) = (\text{C(mg/L)} * \text{a})/(\text{V(ml)}/1000)$$

*The selectivity study of resins toward metal ions*

The produced resins' selectivity toward the elemental ions was investigated using standard solutions (100 ppm) at the maximum treatment duration (often 24 hours) and the maximum acidity function of the metal ion solution, where the ion dissolves rather than precipitates. The temperature was fixed to that of the laboratory. When researching the selectivity of chelating resins toward metal ions, these conditions are frequently employed. The absorbance of the metal ion in the filtrate was then measured after the solutions had been filtered. It is possible to determine whether or not the ion has bonded with the resin by comparing the absorbance values of the ion in the filtrate with its value in the standard solution. The ion and resin have formed a bond if there is a noticeable difference between the two values;

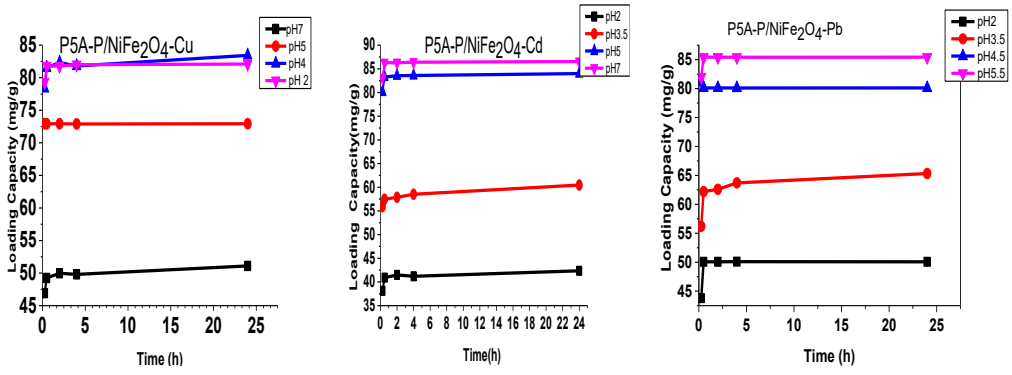


Fig. 16. The impact of treatment duration on the resin loading capacity (P5A-P/$NiFe_2O_4$) for $Pb^{+2}$, $Cd^{+2}$ and $Cu^{+2}$ ions at varying pH is examined.



CC BY

this is part of the analytical study. The bond has not formed, though, if the two values are close, in which case they are not included in the analytical study.

*Study analytical efficiency of the polymer (P5A-P/$NiFe_2O_4$)*

The analytical efficiency of the polymer (P5A-P/$NiFe_2O_4$) against many ions, such as $pb^{2+}$, $Cu^{2+}$, and $Cd^{2+}$, was investigated in this work using the batch method. After shaking 10 milliliters of the investigated ion solution containing 100 parts per million with 0.01 grams of the polymer for 24 hours, the concentration of ions in these solutions was ascertained using flame atomic absorption spectroscopy. The ions $Cu^{2+,}$ $pb^{2+}$, and $Cd^{2+}$ responded well to the polymer.

*First: the impact of treatment duration on the polymer's maximum loading capacity(P5A-P/$NiFe_2O_4$)*

It was investigated how treatment duration affected the polymer [P5A-P/$NiFe_2O_4$]'s loading effectiveness in removing the ions of the elements under study. It was observed that the loading capacity of the polymer rises as the treatment duration for the investigated ion solutions increases. After 0.5 hours, the ions $Pb^{2+}$, $Cu^{2+}$, and $Cd^{2+}$ enter equilibrium, and the loading capacity increases only slightly until the treatment is finished, which is 24 hours later. The impact of treatment duration on the polymer [P5A-P/$NiFe_2O_4$] loading capacity for the ions ($Cd^{2+}$, $pb^{2+}$, and $Cu^{2+}$) in the investigated acidic functions is depicted in Fig. 16.

*Second: the impact of the acid function on the resins' [P5A-P/$NiFe_2O_4$] analytical efficiency is as follows*

It was investigated how the acid function affected the polymer [P5A-P/$NiFe_2O_4$]'s loading efficiency in removing element ions. The acid function study's findings show that the resin P5A-P/$NiFe_2O_4$'s effectiveness toward the ions under investigation is arranged as follows: $Pb^{+2}$ > $Cd^{+2}$ > $Cu^{+2}$ (Fig. 17).

One of the key elements in the adsorption of metal ions on chelated polymers is pH, which is determined by the adsorbents in various acidic solutions. Depending on the pH of the solution, the active functional groups on the nano-adsorbent's surface can be protonated. For our P5A-P $NiFe_2O_4$/nano-resin, it is evident that the adsorption capacity values rise as the pH rises; however, a pH increase above 7 may result in the precipitation of metal ions, which would impede the adsorption process. Because of the competitive adsorption between metal ions and hydronium ions, heavy metal ions have a relatively poor. furthermore, because of the increased concentration of hydronium ions, which decreases the number of binding sites for metal ions, the surfaces of the nano-adsorbents seem to be positively charged. $Cu^{+2}$, $Cd^{+2}$, and $Pb^{+2}$ adsorption on the resin surface was shown to be low in acidic solutions and to increase with pH, with the highest ion adsorption occurring at a pH of around 6. It was shown that the active nitrogen atoms in the resin are essentially largely protonated

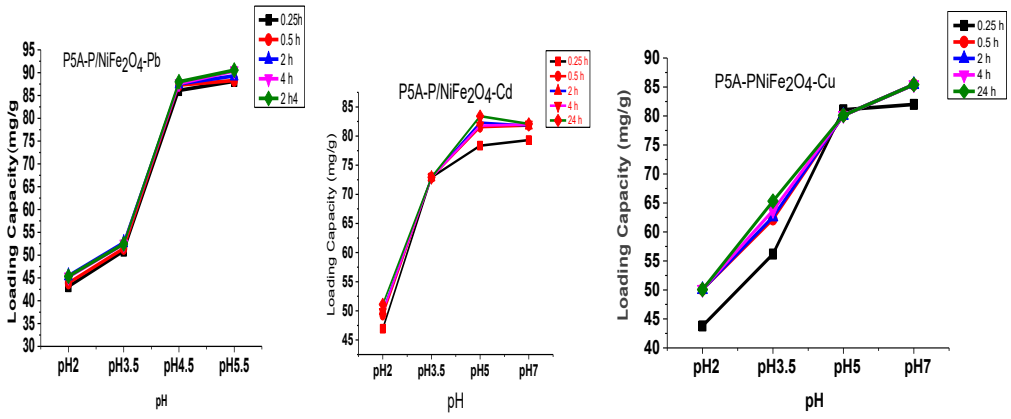


Fig. 17. Impact of pH on resin (P5A-P/$NiFe_2O_4$) loading capacity for $Pb^{2+}$, $Cd^{+2}$ and $Cu^{+2}$ ions at various treatment intervals.



CC BY

when the adsorption values of element ions fall at pH values below 4. Put differently, at low pH levels, $H^+$ ions compete with heavy metal ions for adsorption sites, and positively charged ions and active protons are electrostatically repelled. This restricts the capacity to absorb elements, while the hydrolysis process increases the adsorption of elements when the nitrogen atom is not protonated.

The presence of electron donor atoms, such as oxygen in $OH^-$ and nitrogen in both the amide and azomethine groups, is noteworthy in relation to the adsorption mechanism because they can give a portion of their electron density in the pi system (pi sequence) through resonance. The existence of the delocalized pi electrons in the ligand, which impacts the bonding structure's capacity to complex (chelate), has a significant impact. We may say that the nitrogen atoms in the azomethine group and the oxygen atoms in the hydroxyl group are responsible for the complex formation process. The surface charge has a crucial role in determining how the adsorbents and metal ions interact. Consequently, pH When the charge changes from positive to negative depending on the pH, ZPC is the proper surface indication. The ZPC pH was measured using the salt addition method, which involved preparing multiple samples of 0.1 M

$KNO_3$ solution at varying PHs (2.0–12.0) and stirring them for 24 hours after adding 10 mg of the absorbent material. The pH was then measured once again. Finding each resin's zero charge point (PHZPC), which can be found on the pH chart and expressed by graphing the curve of the change in pH values (PH2-PH1) and expressing it against the initial pH values, is very helpful in determining the optimal pH values for the adsorption of elements.

It was discovered that the ZPC resins for P5A-P/$NiFe_2O_4$ had a pH of roughly 3.4. Thus, we deduce that when the acid function is less than pH < pH ZPC, the proton causes the adsorbent's surface to become positively charged. As a result, the metal ions are electrostatically repelled from the protonated adsorbent's positively charged surface. Protons can also occupy the coordination site on the adsorbents' surface when the pH is less than pH ZPC. The adsorption efficiency of pH < pH ZPC consequently dropped considerably, and it was found that the adsorbent's charge would be negatively charged at low pH values (PH> pH ZPC). This suggests that element ions accumulate at values higher than pH Z values, and that hydroxide will precipitate as pH values rise, extending the

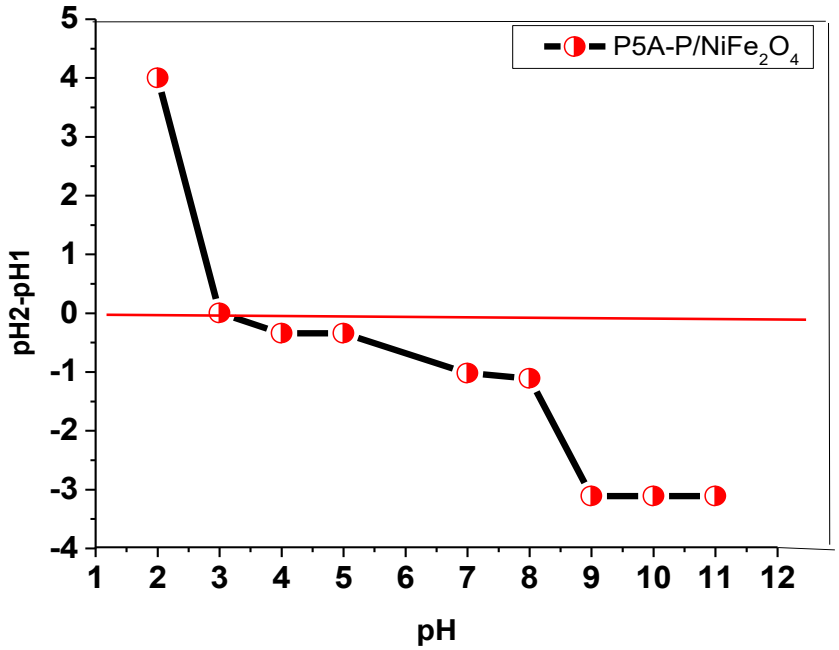


Fig. 18. PHPZP for P5A-P/$NiFe_2O_4$ resins.


CC BY

pH's neutral charge [30,31]. Fig. 18.

*Adsorption Isotherms*

The adsorption of lead, cadmium, and copper ions from aqueous solutions was studied using a prepared polymer surface at temperatures of 25, 35, and 45°C. The relationship between the adsorption capacity (Qe) and the equilibrium concentration (Ce) was plotted to obtain the general form of the adsorption isotherms, as shown in Fig. 19.

Studying adsorption isotherms provides important information in describing the adsorption process and its conditions, as well as determining the adsorption capacity of the adsorbent and its concentration at the time of adsorption. The general shape of the adsorption isotherms of selected heavy metal ions in aqueous media on the surfaces of P5A-P/$NiFe_2O_4$ resin show that they are symmetrical in shape. This indicates that the specific mechanisms of adsorption and absorption remain the same with changes in the system's temperature.

It also appears that it follows group (1) of type (C) according to the classification of (Giles) This indicates the existence of a constant partition between the adsorbent on one hand and the solution and adsorbat on the other, and indicates a high probability of chemical adsorption, and gives rise to substances that penetrate faster than the rate of penetration of the solvent into the adsorbent.

The Langmuir isotherm equation was applied to the experimental data for the adsorption of lead (II), cadmium, and copper ions at temperatures of 25, 35, and 45°C on the prepared P5A-P polymer surface, by plotting Ce/Qe versus Ce, we obtain a straight line with a slope equal to (1/Qm) and an intercept equal to (1/Qmb), from which the maximum adsorption capacity (Qmax), the Langmuir constant (b) , the correlation coefficient ($R^2$) was calculated , this is a distinctive features of the Langmuir isothermisotherm [32].

The Freundlich isotherm equation was applied to experimental data for the adsorption of lead (II), cadmium (II),, and copper (II), ions onto polymer surfaces at temperatures of 25, 35, and 45°C. The linear form of the Freundlich equation for the

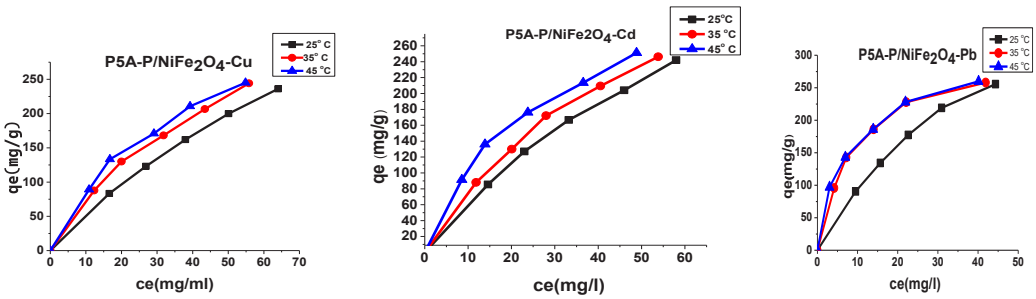


Fig. 19. Adsorption isotherms of $Pb^{+2}$, $Cd^{+2}$, $Cu^{+2}$ ions on the surface of P5A-P/ Ni $Fe_2O_4$ at different temperatures.

Table 2. Shows the values of the Langmuir Freundlich constant (b), the maximum adsorption capacity (Qm), and the correlation coefficient ($R^2$) for the adsorption of heavy metal ions onto the surface of P5A-P/$NiFe_2O_4$composite at different temperatures.

| | | Langmuir isotherm | | | Freundlich Isotherm | | |
|---|---|---|---|---|---|---|---|
| Metal ions | T °C | Qm mg/g | b | $R^2$ | n | kf | R2 |
| Pb | 25 | 526.315 | 0.0223 | 0.9904 | 1.1655 | 20.007 | 0.9885 |
| | 35 | 312.5 | 0.10958 | 0.9987 | 2.3452 | 57.305 | 0.9546 |
| | 45 | 303.030 | 0.13314 | 0.9961 | 2.5733 | 65.539 | 0.9869 |
| Cd | 25 | 588.235 | 0.011707 | 0.9915 | 1.3415 | 11.915 | 0.9957 |
| | 35 | 500 | 0.017969 | 0.9926 | 1.4634 | 16.6916 | 0.9926 |
| | 45 | 384.615 | 0.03703 | 0.9909 | 1.7937 | 29.2886 | 0.9846 |
| Cu | 25 | 666.666 | 0.0085 | 0.9962 | 1.2913 | 9.5741 | 0.9991 |
| | 35 | 476.190 | 0.01815 | 0.9834 | 1.5085 | 17.060 | 0.9956 |
| | 45 | 416.666 | 0.02575 | 0.9828 | 1.6420 | 21.872 | 0.9817 |



CC BY

adsorption of lead (II), cadmium, and copper ions onto polymer surfaces by plotting Log Qe versus LogCe, we obtain a straight line with a slope equal to 1/n and an intercept equal to log KF, from which the Freundlich constant (Kf) was calculated. The correlation coefficient ($R^2$) was also calculated, and its values are shown in Table 2. It was observed from the tables that all values of n/1 fall within the range 0< 1/n < 1. This indicates that all adsorption processes are Polymeric surfaces were preferred and feasible in this study.

The Qm values obtained from applying the Langmuir model to the studied adsorption system may not reflect the actual operational Qm value within the studied concentration range, but rather represent a theoretical adsorption capacity resulting from a mathematical induction process. However, the Freundlich model gives a more realistic description of the adsorption process, where values of the constant n greater

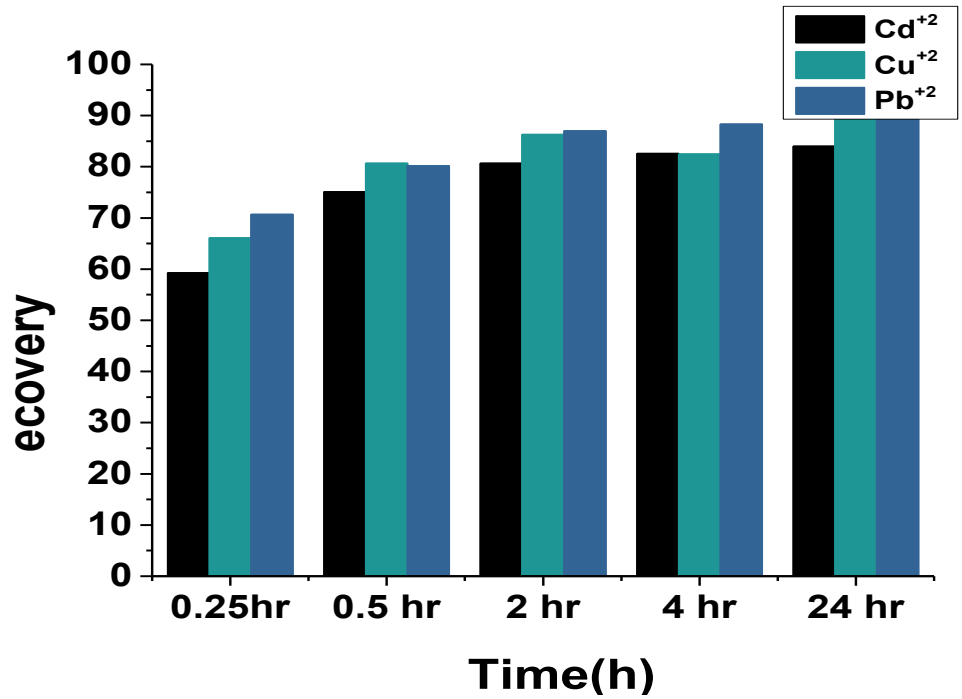


Fig. 20. Percentage recovery of ions from the loaded resin (P5A-P/$NiFe_2O_4$) at different times.

Table 3. Adsorption parameters according to Pseudo first order and Pseudo second order.

| Adsorbate | Pseudo-first-order kinetic model | | | | Pseudo- second-order kinetic model | | | |
|---|---|---|---|---|---|---|---|---|
| | $q_{(exp)}$ (mg/g) | $R^2$ | $Q_{(exp)}$ (mg/g) | K1 | $q_{(exp)}$ (mg/g) | $R^2$ | $Q_{(exp)}$ (mg/g) | K2 |
| Pb | 90.5 | 0.9543 | 17.054 | 0.0927 | 90.5 | 0.9995 | 93.458 | 0.89 |
| Cd | 86.5 | 0.93 | 13.817 | 0.0851 | 86.5 | 0.9993 | 90.09 | 0.74 |
| Cu | 83.4 | 0.9551 | 8.588 | 0.0701 | 83.4 | 0.9993 | 85.47 | 1.1037 |


CC BY

than one indicate preferential adsorption on a heterogeneous surface containing adsorption sites with varying energies.

The adsorption rate, which is the time required to reach equilibrium in the adsorption process, is determined by the adsorption kinetics. Kinetic models can be used to explain the adsorption mechanism and the mechanisms that control its potential rate. To study the adsorption kinetics of metal ions onto the prepared resin, first- and second-order pseudo-models were used. [5,24,33].

*Pseudo-First-Order Model*

The pseudo-first-order kinetics diagrams for every ion on the produced resin at 25°C are displayed. The computed adsorption rate constants K1, maximum adsorption capacity Q, and correlation coefficient R2 for the pseudo-first-order kinetics model are displayed in Table 3. Plotting ln(qe-qt) against (t) yielded these values; the values of K1 and Q are found in the diagram's slope and intercept.

*Pseudo-Second-Order Model*

The pseudo-second-order equations for adsorption system onto produced resin at (25) °C. The values of the computed adsorption rate constants $K^2$, maximum adsorption capacity Q, and correlation coefficient $R^2$ for the pseudo-second-order model are shown in Table 3 a. These values were derived from the plot of (t/qt) against (t); the slope and intercept of the plot yield the values of $K^2$ and Q.

The major adsorption mechanism and response rate for lead ($Pb^{2+}$), cadmium ($Cd^{2+}$), and copper ($Cu^{2+}$) ions were identified by analyzing the experimental data and modeling the adsorption kinetics using pseudo-first-order and pseudo-second-order models. The calculated values of the adsorption capacity at equilibrium qe from the pseudo-second-order model (93.458, 89.09, and 85.47 mg $g^{-1}$ for Pb, Cd, and Cu, respectively) showed high agreement with the experimental values, confirming the accuracy of this model in representing the data. The linear regression results between the calculated and experimental values revealed that the pseudo-second-order model provided the best agreement with the experimental data for all studied ions, with coefficients of determination ($R^2$) ranged from 0.93 to 0.9551 for the pseudo-first-order model.

These findings show that chemistry largely controls the adsorption process, with the adsorption rate being more dependent on the interaction between the active sites on the adsorbent surface and the adsorbed molecules than it is on the concentration in the solution [33,34].

The results proved that the pseudo-second-order kinetic model is the most suitable for representing adsorption behavior, as evidenced by the good agreement between the calculated and experimental values of adsorption capacity, these results indicate that the rate control step is subject to a chemical reaction, and this interpretation is consistent with the more realistic description provided by the Freundlich model without contradicting the surface heterogeneity reflected by the Freundlich model.

*Recovery of metal ions from loaded resin*

The activation process of the resin was studied in the direction of the ions ($pb^{2+}$, $Cu^{2+}$, $Cd^{+2}$) when the treatment time with HCl increased, the percentage of recovery increased as in Fig 20. The study's findings suggest that the recovery percentage increases with increasing time and that the highest recovery percentage was 24 hours and according to the following arrangement of ions for the P5A-P/$NiFe_2O_4$ resin.

This work investigated the recovery of heavy metal ions from saturated resins after activation with a hydrochloric acid (HCl) solution at a specific concentration. The aim was to evaluate the effect of acid treatment time on the recovery efficiency of the metal ions: lead ($Pb^{2+}$), copper ($Cu^{2+}$), and cadmium ($Cd^{2+}$).

Experimental results, as shown in Fig. 20, showed that increasing the hydrochloric acid treatment time led to a gradual increase in the ion recovery rates from the resins. This behavior can be explained by enhanced ion exchange between hydrogen ions in the acidic medium and metal ions bound to active groups within the resin structure, such as carboxyl (–COOH) or amine ($–NH_2$) groups. Over time, the number of available active exchange sites increases, contributing to the dissociation of metal ions from the resin and improving recovery efficiency

The highest recovery rate was achieved after 24 hours of treatment, indicating that the system reached near-equilibrium between the ions in the


CC BY

solution and those adsorbed on the resin surface. The results also showed that the order of recovery efficiencies for the ions followed the sequence:

$Pb^{2+} > Cu^{2+} > Cd^{2+}$

This order can be explained based on the ion's physical and chemical properties, including ionic radius, hydration energy, and stability constant for complexation with functional groups. The lead ion has a larger ionic radius and a greater ability to interact with active groups than copper and cadmium ions, resulting in a relatively higher recovery.

From a kinetic modeling perspective, the results indicate that the process mechanism can be described by two sequential models: film diffusion, where metal ions migrate from the liquid layer surrounding the resin particle to its outer surface intraparticle diffusion, where ions penetrate the internal pore network to reach the active exchange sites.

In the early stages of treatment, the recovery rate is limited by the external diffusion phase, while the effect of internal diffusion increases over time until equilibrium is reached. This observation is consistent with the pseudo-second-order kinetic model, which indicates that the rate-determining step of the process depends on chemical interactions between ions and the active sites rather than a purely diffusional process.

These results indicate that the acid treatment time is a critical factor in improving the recovery efficiency of metal ions from loaded resins.

Further studies are recommended to evaluate the effect of acid concentration, temperature, and resin to solution volume ratio, as well as to fit the data with multiple kinetic models (Langmuir, Freundlich) to more accurately determine the adsorption and separation mechanism and achieve the maximum possible recovery efficiency while maintaining the integrity of the resin polymer structure [26].

## CONCLUSION

In conclusion, azomethine amide P5A-P resin was grafted onto superparamagnetic $NiFe_2O_4$ nanoparticles produced by the co-precipitation process to produce a type of polymer composite material with an exceptional magnetic response. Some of the structural and morphological characteristics were assessed using X-ray diffraction (XRD), transmission electron microscopy (TEM), and vibrating sample magnetization (VSM). The uses of the produced magnetic particle-based composite resin for the removal of Cu (II), Cd (II), and Pb (II) ions from wastewater were investigated in addition to the resin's characterization using various spectroscopic techniques. Two factors that influence adsorption, contact time and pH, were also examined. One of the most promising methods for removing metal contaminants from aqueous solutions is magnetic chelating polymer separation. Importantly, the discovery presents a new family of magnetically separable chelating polymers that combine the easy magnetic recoverability of $NiFe_2O_4$ nanoparticles with the powerful binding ability of azomethine-based ligands. In addition to improving adsorption effectiveness and reusability, this hybrid approach provides a scalable, economical, and environmentally friendly method for removing heavy metals from aqueous systems. Thus, the created substance is a potential development in the field of magnetic nanocomposite adsorbents for environmental cleanup.

## CONFLICT OF INTEREST

The authors declare that there is no conflict of interests regarding the publication of this manuscript.

## REFERENCES

1. Shui L, Pan X, Chen X, Chang F, Wan D, Liu D, et al. Pollution Characteristics and Ecological Risk Assessment of Heavy Metals in Sediments of the Three Gorges Reservoir. Water. 2020;12(6):1798.
2. Comparative Study of the Extraction of Cu(II) and Fe(II) Ions Using Chitosan and Modified Chitosan/Polyvinylpyrrolidone Adsorptive Membranes: Adsorption, Kinetic, and Thermodynamic Study. American Chemical Society (ACS). http://dx.doi.org/10.1021/acsapm.3c00727.s001
3. Μυρόβαλη Ε. Magnetic nanoparticle arrays: National Documentation Centre (EKT).
4. Hakeem HS, Abbas NK. Preparing and Studying Structural and Optical Properties of Pb1-xCdxS Nanoparticles of Solar Cells Applications. Baghdad Science Journal. 2021;18(3):0640.
5. iaset I. Preparation of Activated Carbon from Reed Phragmites Australis (Cav.) and A Study Of Its Effectiveness in Adsorption of Malathion. SSRN Electronic Journal. 2021.
6. Bustamante-Torres M, Romero-Fierro D, Arcentales-Vera B, Pardo S, Bucio E. Interaction between Filler and Polymeric Matrix in Nanocomposites: Magnetic Approach and Applications. Polymers. 2021;13(17):2998.
7. Murugesan A, Ravikumar L, SathyaSelvaBala V, SenthilKumar P, Vidhyadevi T, Kirupha SD, et al. Removal of Pb(II), Cu(II) and Cd(II) ions from aqueous solution using polyazomethineamides: Equilibrium and kinetic approach.


CC BY

Desalination. 2011;271(1-3):199-208.
8. Reglero Ruiz J, Trigo-López M, García F, García J. Functional Aromatic Polyamides. Polymers. 2017;9(9):414.
9. Powell CD, Atkinson AJ, Ma Y, Marcos-Hernandez M, Villagran D, Westerhoff P, et al. Magnetic nanoparticle recovery device (MagNERD) enables application of iron oxide nanoparticles for water treatment. J Nanopart Res. 2020;22(2).
10. Mishurov D, Voronkin A, Nedilko O, Zykina I. The influence of different factors on exploitation properties of nonlinear optical polymeric materials based on an epoxy matrix doped with flavonoids. Polym Test. 2020;87:106535.
11. Shi X, Ding Z, Wang C, Song S, Zhou X. Effect of different cellulose polymers on the crystal growth of celecoxib polymorphs. J Cryst Growth. 2020;539:125638.
12. Al-Sabagh AM, Moustafa YM, Hamdy A, Killa HM, Ghanem RTM, Morsi RE. Preparation and characterization of sulfonated polystyrene/magnetite nanocomposites for organic dye adsorption. Egyptian Journal of Petroleum. 2018;27(3):403-413.
13. Zhu N, Ji H, Yu P, Niu J, Farooq MU, Akram MW, et al. Surface Modification of Magnetic Iron Oxide Nanoparticles. Nanomaterials. 2018;8(10):810.
14. Khan I, Saeed K, Khan I. Nanoparticles: Properties, applications and toxicities. Arabian Journal of Chemistry. 2019;12(7):908-931.
15. Khalaj M, Khatami S-M, Kalhor M, Zarandi M, Anthony ET, Klein A. Polyethylenimine Grafted onto Nano-NiFe2O4@SiO2 for the Removal of $CrO_4^{2-}$, $Ni^{2+}$, and $Pb^{2+}$ Ions from Aqueous Solutions. Molecules. 2023;29(1):125.
16. Fadhel SR. Chitosan-NiFe2O4 Nanocomposite Synthesis for Effective Removal of Pb(II) and Zn(II) from Aqueous Solution. Results in Engineering. 2024;24:103293.
17. Satyanarayana Acharyulu NP, Sohan A, Banoth P, Chintalapati S, Doshi S, Reddy V, et al. Effect of the Graphene- Ni/$NiFe_2O_4$ Composite on Bacterial Inhibition Mediated by Protein Degradation. ACS Omega. 2022;7(35):30794-30800.
18. Recent Advances of Using Polymer Nanocomposites For the Removal of Heavy Metal Ions From Waste Water: A Review. Global NEST Journal. 2025.
19. Kong X, Li F, Li Y, He X, Chen L, Zhang Y. Molecularly imprinted polymer functionalized magnetic $Fe_3O_4$ for the highly selective extraction of triclosan. J Sep Sci. 2019;43(4):808-817.
20. Zhang L-J, Qi L, Chen X-Y, Liu F, Liu L-J, Ding W-L, et al. Synthesis, Crystal Structure and Photophysical Properties of Two Reduced Schiff Bases Derived from 5-Aminoisophthalic Acid. J Chem Crystallogr. 2018;49(4):260-266.
21. Wei S, Zhu Y, Zhang Y, Xu J. Preparation and characterization of hyperbranched aromatic polyamides/Fe3O4 magnetic nanocomposite. React Funct Polym. 2006;66(11):1272-1277.
22. Santiago AA, Ibarra-Palos A, Cruz-Morales JA, Sierra JM, Abatal M, Alfonso I, et al. Synthesis, characterization, and heavy metal adsorption properties of sulfonated aromatic polyamides. High Perform Polym. 2017;30(5):591-601.
23. Farounbi AI, Mensah PK, Olawode EO, Ngqwala NP. 1H-NMR Determination of Organic Compounds in Municipal Wastewaters and the Receiving Surface Waters in Eastern Cape Province of South Africa. Molecules. 2020;25(3):713.
24. Bashir AKH, Matinise N, Sackey J, Kaviyarasu K, Madiba IG, Kodseti L, et al. Investigation of electrochemical performance, optical and magnetic properties of NiFe2O4 nanoparticles prepared by a green chemistry method. Physica E: Low-dimensional Systems and Nanostructures. 2020;119:114002.
25. Goutam SP, Saxena G, Singh V, Yadav AK, Bharagava RN, Thapa KB. Green synthesis of TiO2 nanoparticles using leaf extract of Jatropha curcas L. for photocatalytic degradation of tannery wastewater. Chem Eng J. 2018;336:386-396.
26. Yousef A Al Dalahmeh YAAD, Fawwaz I Khalili FIK, Bassam A Sweileh BAS. Synthesis, Characterization of Poly(1,4–cyclohexanedimethylene oxalate) and the Study of its Metal Uptake Behavior Towards Pb(II), Zn(II), and Cd(II) Ions. J Chem Soc Pak. 2019;41(3):421-421.
27. Kalsoom A. AN INTEGRATED APPROACH FOR SAFE REMOVAL OF CHROMIUM (VI) BY BREVIBACTERIUM SP. Pakistan Journal of Science. 2022;72(1).
28. Grozdanov A, Atkovska K, Lisickov K, Ruseska G, Dimitrov AT. Removal of Heavy Metal Ions from Wastewater Using Bio- and Nanosorbents. Springer Water: Springer International Publishing; 2017. p. 239-244. http://dx.doi.org/10.1007/978-3-319-71279-6_33
29. Mallakpour S, Khadem E. Carbon Nanotubes for Heavy Metals Removal. Composite Nanoadsorbents: Elsevier; 2019. p. 181-210. http://dx.doi.org/10.1016/b978-0-12-814132-8.00009-5
30. Fu J, Wang X, Li J, Ding Y, Chen L. Synthesis of multi-ion imprinted polymers based on dithizone chelation for simultaneous removal of $Hg^{2+}$, $Cd^{2+}$, $Ni^{2+}$ and $Cu^{2+}$ from aqueous solutions. RSC Advances. 2016;6(50):44087-44095.
31. Ali O, Mohamed S. Adsorption of copper ions and alizarin red S from aqueous solutions onto a polymeric nanocomposite in single and binary systems. TURKISH JOURNAL OF CHEMISTRY. 2017;41:967-986.
32. Health hazard evaluation report: HETA-91-003-2232, Scott Molders, Inc., Kent, Ohio. U.S. Department of Health and Human Services, Public Health Service, Centers for Disease Control, National Institute for Occupational Safety and Health; 1992 1992/07/01.
33. Akkaya R. Removal of radioactive elements from aqueous solutions by adsorption onto polyacrylamide–expanded perlite: Equilibrium, kinetic, and thermodynamic study. Desalination. 2013;321:3-8.
34. Youssif MM, Wojnicki M. Efficacious Removal of $Cd^{2+}$ and $Pb^{2+}$ Ions from Wastewater Using a Novel $Fe_3O_4/SiO_2$/PANI-SDBS Nanocomposite. Materials. 2025;18(9):2083.



CC BY